Acta Pharmaceutica Sinica B 2025;15(5):2625−2639

Chinese Pharmaceutical Association
Institute of Materia Medica, Chinese Academy of Medical Sciences

Acta Pharmaceutica Sinica B

www.elsevier.com/locate/apsb
www.sciencedirect.com

ORIGINAL ARTICLE

A proximity-induced chimera platform for targeted protein arginine methylation

Yanlin Jian[†], Tianyang Zhou[†], Chendong Guo[†], Yibo Gao, Chen Yao, Zixi Wang, Xuehan Jiang, Ke Wang, Jian Ma, Yang Gao, Yizeng Fan, Jing Liu, Bohan Ma[*], Lei Li[*]

Department of Urology, the First Affiliated Hospital of Xi'an Jiaotong University, Xi'an 710061, China

Received 10 August 2024; received in revised form 13 February 2025; accepted 12 March 2025

KEY WORDS

Protein arginine methyltransferases;
Arginine methylation;
Bifunctional molecules;
Methylation tagging system;
Ternary complex;
Androgen receptor;
AKT;
P300

Abstract Arginine methylation is a critical post-translational modification that plays multifaceted biological functions. However, the manipulation of protein arginine methylation largely depends on genetic or pharmaceutic inhibition of the regulatory enzymes, protein arginine methyltransferases (PRMTs), or non-methylation substitution of corresponding arginine residue to lysine or alanine of protein of interest (POI), which inevitably affects other substrates, or disrupts the structure of POI. Thus, it urges an approach to specifically modulate the arginine methylation of a POI under physiological conditions. To this end, we report the discovery of a methylation tagging system (MeTAG), that enables targeted modification of protein arginine methylation. Through bridging the methyltransferase PRMT5 proximity to a POI, MeTAG facilitates the arginine methylation of POIs, including known arginine methylated proteins, androgen receptor (AR) and protein kinase B (AKT), as well as a neo-substrate E1A binding protein (p300), in a reversible and PRMT5-dependent manner. Moreover, MeTAG can regulate downstream signaling in a methylation dependent manner, leading to downregulation of *PSMA* mRNA level and activation of AKT. Therefore, MeTAG represents a feasible approach to modulate protein methylation and thereby perturbs protein function in biological and therapeutic contexts.

*Corresponding authors.
E-mail addresses: lilydr@163.com (Lei Li), bohanma1222@gmail.com (Bohan Ma).
[†]These authors made equal contributions to this work.

Peer review under the responsibility of Chinese Pharmaceutical Association and Institute of Materia Medica, Chinese Academy of Medical Sciences.

https://doi.org/10.1016/j.apsb.2025.03.049

1. Introduction

Protein arginine methylation involves the transfer of a methyl group from the methyl donor *S*-adenosylmethionine (SAM) to the guanidinium group of arginine[1,2], and has been identified on over 4000 proteins, including histones and non-histone substrates[3−5]. Arginine methylation has been implicated in a wide array of biological processes including transcription, signal transduction, DNA damage response, RNA translation, and protein stability[3,6−8]. Despite its contribution to drive cellular process, dysregulation of arginine methylation by protein arginine methyltransferases (PRMTs) is involved in numerous diseases including cancer[3,9], neurodegenerative diseases[10,11] and inflammatory diseases[12]. Thus, precise manipulation of methylation on a protein of interest (POI) stands as a prerequisite for deepening our comprehension of the biological mechanisms underlying protein methylation. Subsequently, it paves the way for therapeutic interventions targeting this process. To this end, genetic approaches and chemical probes approaches have emerged, including methylarginines antibodies, advanced proteomic techniques and small molecule probes, making research on arginine methylation possible. While the arginine-to-lysine (R-to-K) or alanine (R-to-A) mutations are used as non-methylation mutation, the arginine-to-phenylalanine (R-to-F) methylation-mimetic mutation is still under debate[13], thus posing obstacles in biological research. On the other hand, chemical probes targeting PRMT enzymes though have spurred significant transformative impact in basic life science and translational medicine, PRMT inhibition inevitably introduces side-effect toxicity due to global changes in substrates methylation, since each PRMT enzyme is typically responsible for hundreds of protein substrates, undermining their translational value. In addition, several inhibitors targeting arginine demethylases, including deaminase enzymes peptidyl arginine deaminase 4 (PAD4)[14−16], Jumonji domain-containing protein 6 (Jmjd6)[17−19], and a subset of Jumonji C domain histone lysine demethylases (JmjC KDMs)[20] have been developed, contributing to the increasing arginine methylation level. However, such molecules simultaneously disturb other cellular process, *e.g.* lysine methylation, since these proteins are multifunctional. Besides, similar to PRMT inhibitors, a global methylation level alteration is induced by arginine demethylase inhibitors due to the broad range of substrates of these proteins. Altogether, small molecules that selectively modulate methylation on POIs in cells without inducing global alterations to substrates are still limited and urgently needed. Such small molecules would prove advantageous in various scenarios due to their capacity to explore unknown proteins subjected to arginine methylation. Moreover, they possess the potential to initiate cell-signaling events, overcoming challenges often encountered with conventional methodologies, and thus to provide an alternative strategy to intervene diseases.

There are three types of arginine methylation, including monomethylation, asymmetric dimethylation, and symmetric dimethylation, which are catalyzed by different PRMTs. Type I PRMTs[7], consisting of PRMT1-4, PRMT6 and PRMT8, are responsible for asymmetric dimethylation of arginine (ADMA), type II PRMTs, PRMT5[21] and PRMT9[22], are for symmetric dimethylation of arginine (SDMA), while the only type III enzyme, PRMT7[23], is for monomethylation of arginine (MMA). Among them, PRMT1 and PRMT5 have been emerged as valuable therapeutic targets in various cancers, particularly in patients with methylthioadenosine phosphorylase gene (MTAP) loss[3,9,24], and their inhibitors are now in clinical trials[25−27]. However, PRMTs are also critical for the survival of non-carcinoma cells, as Prmt1 and Prmt5 null mice are embryonic lethal[3,28]. Therefore, it urges the precise dissection of methylated proteins between cancer cells and non-carcinoma cells using tool that can specifically manipulate arginine methylation on the POI while sparing other PRMT substrates.

Heterobifunctional molecules have been reported to bring an enzymatic protein close to the POI to induce ubiquitination/deubiquitination[29,30], phosphorylation/dephosphorylation[31,32], acetylation[33], and *O*-glycosylation[34,35], but there is still a lack of tool to introduce arginine methylation onto POIs. In this study, we designed heterobifunctional molecules, termed as methylation tagging system (MeTAG), to selectively and dynamically introduce arginine methylation on POIs. Through the two warheads to recruit PRMT5 and POI individually, MeTAG induces proximity to facilitate the arginine methylation of POI (Fig. 1A). Taken two known arginine methylation substrates, androgen receptor (AR) and protein kinase B (AKT), as examples, MeTAGs induced their symmetric dimethylation in a PRMT5-dependent manner, thus inhibiting AR signaling and activating AKT signaling,

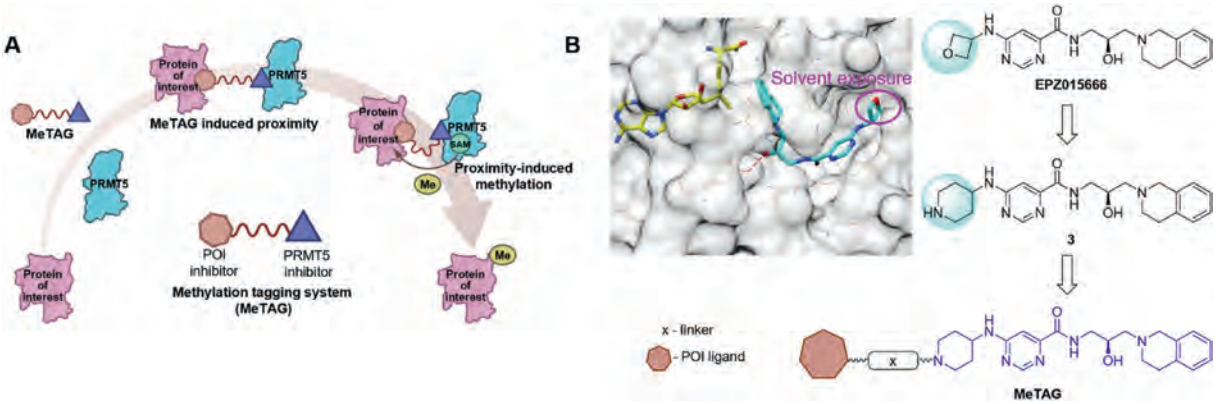

Figure 1 Development of MeTAG system to enable arginine methylation on a protein of interest (POI). (A) Schematic diagram of MeTAG system consisting of PRMT5 and POI warheads, which bridges PRMT5 and POI into proximity to facilitate PRMT5-mediated arginine methylation on the POI. (B) Ligand design for PRMT5 binding. Left: co−crystal structure of PRMT5:MEP50 (light gray) in complex with EPZ015666 (cyan) and its substrate SAM (yellow, PDB: 4X61). Right: chemical structures of EPZ015666, piperidine replaced analogue **3**, and designed MeTAG.

respectively, consistent with their previously reported functions[36−38]. In addition, E1A binding protein (p300), a protein yet not being identified as a PRMT5 substrate, was able to be methylated with the heterobifunctional molecule p300-MeTAG **1**. Taken together, the proof-of-concept MeTAG system provides a generalizable way to manipulate the arginine methylation of POIs, and represents a unique research and translational tool to uncover the biological function of protein arginine methylation.

2. Results and discussion

*2.1. Heterobifunctional p300-MeTAG **1** induced PRMT5−AR interaction facilitates arginine methylation of AR*

To induce arginine methylation on a POI, we utilized a reversible uncompetitive PRMT5 inhibitor EPZ015666 as its ligand to develop the MeTAG, which recruits PRMT5 to be close to a POI for the transfer of the methyl group on the target (Fig. 1A). Based on the co−crystal structure of PRMT5:MEP50 in complex with EPZ015666, the oxetane moiety on EPZ015666 protruded out to solvent and barely showed any interactions with PRMT5 structure (Fig. 1B)[39], thus being an optimal attachment point for linker binding. In another PRMT5 inhibitor in clinical trial, GSK3326595, the oxetane moiety was replaced with a more synthetically amenable piperidine ring[40]. Therefore, we adopted the piperidine ring-replaced compound **3** (Fig. 1B) as PRMT5 ligand for MeTAG development. AR has been reported as a substrate of PRMT5[38], thus we chose AR as the first target protein of MeTAG. For AR recruitment, we used its well-established inhibitor enzalutamide[41] as ligand (Fig. 2A), since it is an ideal warhead for recruiting AR in other chemically induced proximity approaches, such as proteolysis targeting chimera (PROTAC)[42].

Three envisioned AR-MeTAGs were constructed through conjugating PRMT5 binder and hydrolyzed product of enzalutamide with different linkers, *via* two consecutive amidation steps (Supporting Information Fig. S1A and Supporting Information Scheme S1). To gain insight into the putative binding mode, molecular docking and molecular dynamics simulation (MD) were performed for the envisioned AR-MeTAGs. To model the trimer formation process, we anchored the docking structure of one protein to the bifunctional molecule and subsequently docked the second protein. The resulting RMSD curve serves as an indicator for equilibrium, and the structural features of the ternary complex reveal detailed interactions.

Docking indicated that AR-MeTAG **1** is better accommodated than AR-MeTAG **2/3** (Fig. 2B and Supporting Information Fig. S2). Compared with AR-MeTAG **2/3**, AR-MeTAG **1** adopted a more compact conformation to simultaneously bind to AR and PRMT5, thus inducing the formation of the AR: AR-MeTAG **1**: PRMT5 ternary complex. This putative ternary complex induced by AR-MeTAG **1** is supposed to be stable as predicted by MD (Fig. 2C). The capacity of AR-MeTAG to induce physical interaction between AR and PRMT5 was assessed using a fluorescence polarization (FP) assay. Among the three synthesized compounds, AR-MeTAG **1**, but not AR-MeTAG **2/3**, effectively promoted the formation of the ternary complex, with a median concentration of 765.2 nmol/L (Fig. 2D). To further explore the AR: AR-MeTAG **1**: PRMT5 ternary complex formation process, AR protein was incrementally added to AR-MeTAGs solution according to a concentration gradient. For these three AR-MeTAGs, the fluorescence polarization value increased proportionally with the concentration of AR protein, indicating the binding of envisioned AR-MeTAGs to AR protein. Subsequently, with the addition of PRMT5 protein, only the fluorescence polarization value of AR-MeTAG **1** continued to rise and eventually reached a new plateau compared to AR-MeTAG **2** and **3** (Fig. S1B). This progression verifies the formation of the AR: AR-MeTAG **1**: PRMT5 trimer complex, while AR-MeTAG **2** and **3** failed to induce the formation of the trimer complex. Consistent with the *in vitro* binding results, AR-MeTAG **1** also demonstrated its ability to augment the binding between AR and PRMT5 within cellular environments (Fig. 2E). Additionally, AR-MeTAG **1**-induced interaction between AR and PRMT5 could be counteracted by cotreatment with excessive PRMT5 inhibitor GSK3326595 (Fig. 2E). Notably, AR-MeTAG **1** effectively induced the SDMA on AR in 293T that transfected with AR and PRMT5 (Fig. 2F)[38,43], while AR-MeTAG **2** and **3** did not (Fig. S1C and S1D). To further substantiate the dependence of AR-MeTAG **1**-mediated arginine methylation on PRMT5, the prostate cancer VCaP cells were depleted of the endogenous *PRMT5* using short hairpin RNA (shRNA) prior to MeTAG treatment. The results conclusively showed that the SDMA modification of AR induced by AR-MeTAG **1** was abolished in VCaP-shPRMT5 cells (Fig. 2G), indicating the dependence on PRMT5. Considering the warhead of PRMT5 was derived from an inhibitor, we further investigate the inhibitory effect of AR-MeTAG **1** on PRMT5 in C4-2 cells. As shown in Fig. S1E, the relative catalytic activity of PRMT5 remains unchanged after AR-MeTAG **1** treatment, suggesting the negligible effect of AR-MeTAG **1** on PRMT5 in the concentration we used.

*2.2. Arginine methylation induced by AR-MeTAG **1** attenuates the transcriptional function of AR*

According to previous report, endogenous PRMT5 methylates AR and subsequently attenuates AR activity in transcription of *PSA*[38]. Next, we assessed the effect of AR-MeTAG **1** in regulating AR function, using AR target genes, *PSA*, *NKX3.1* and *TMPRSS2*, as biomarkers (Fig. 3A)[44−47]. Quantitative RT-PCR analysis established that AR-MeTAG **1** decreased *PSA* expression in a dose-dependent manner in VCaP cells (Fig. 3B). Conversely, no substantial alteration in *PSA* mRNA level was observed following enzalutamide treatment, even at concentration up to 20 μmol/L (Fig. S1F). These results indicated that AR-MeTAG **1** treatment-induced AR inhibition could not be due to the effect of enzalutamide in directly inhibiting AR. Consistent with previous report[38], *PSA* mRNA level in VCaP-shPRMT5 cells was higher than that in VCaP-shScr cells (Fig. 3C). More importantly, knockdown of *PRMT5* mitigated the inhibitory effect of AR-MeTAG **1** on *PSA* mRNA expression (Fig. 3C), further supporting our notion that AR-MeTAG **1** inhibits AR function in a PRMT5-dependent manner. In addition, wash-out experiment of AR-MeTAG **1** after a 12 h treatment showed a recovery of *PSA* mRNA to basal levels within 12 h, suggesting the AR inhibitory effect is reversible and AR-MeTAG **1** dependent (Fig. 3D).

The effects of AR-MeTAG **1** in reducing the expression of the AR target genes, *PSA*, *TMPRSS2*, and *NKX3.1*, were also validated in another prostate cancer cell line, C4-2 (Fig. 3E−G, Fig. S1G). Moreover, the effect of AR-MeTAG **1** on the proliferation of C4-2 cells was stronger than PRMT5 inhibitor GSK3326595, AR inhibitor enzalutamide, and combination of GSK3326595 and enzalutamide, with an IC_{50} of 9.9 μmol/L (Fig. 4A, Fig. S1H). In the tested concentrations of combined

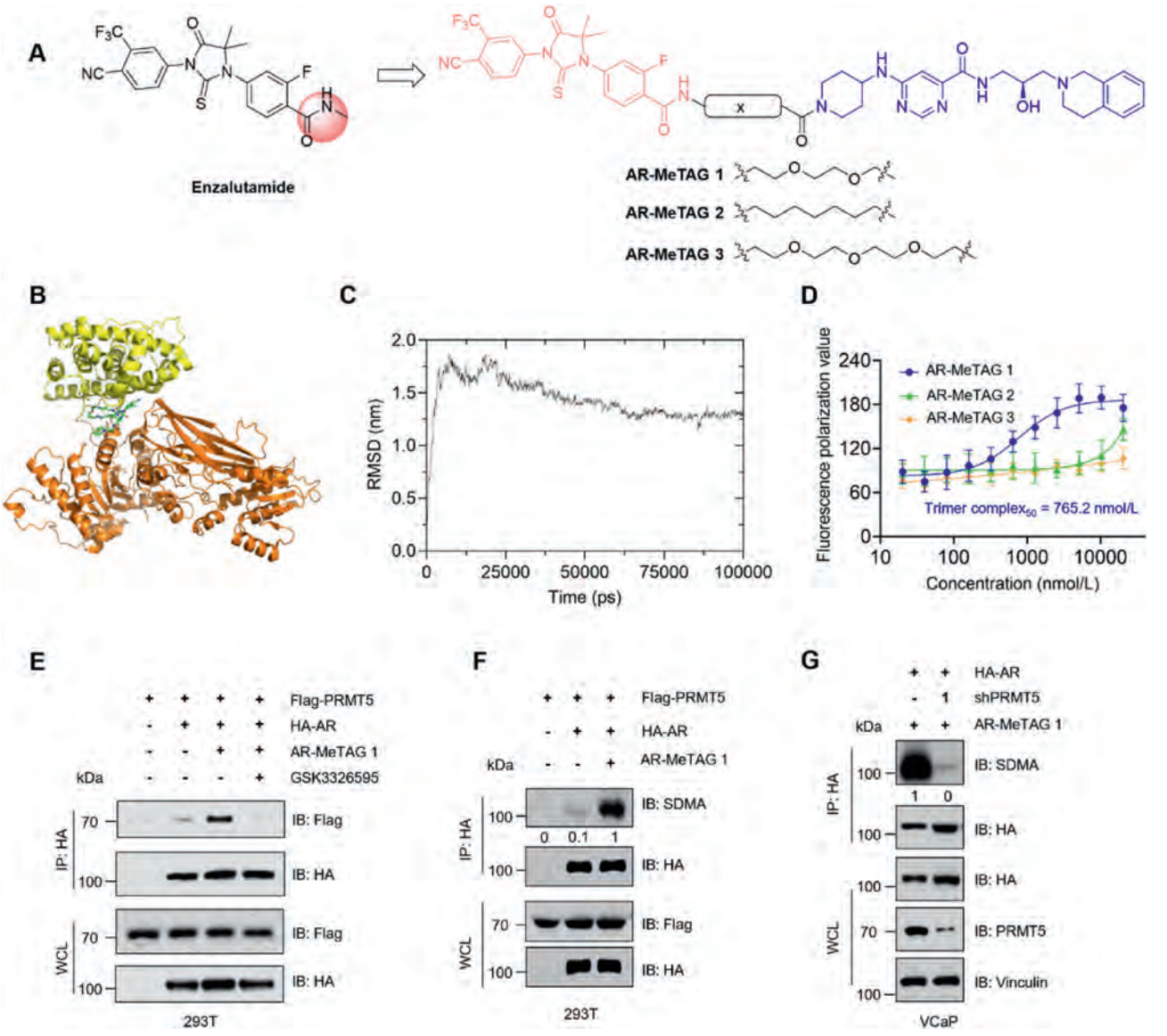

Figure 2 Development of AR-MeTAG system to enable arginine methylation on AR. (A) Schematic diagram of AR-MeTAG system consisting of PRMT5 and AR warheads, which bridges PRMT5 and AR into proximity to facilitate PRMT5-mediated arginine methylation on AR. (B) The predicted binding mode of the AR: AR-MeTAG **1**: PRMT5 ternary complex (yellow: AR, orange: PRMT5). (C) The RMSD curve of the ternary complex. (D) AR-MeTAG molecules induced the formation of AR: AR-MeTAG: PRMT5 complex detected by fluorescence polarization (FP). (E) AR-MeTAG **1** promoted complex formation detected by co-immunoprecipitation (Co-IP) of AR-HA and PRMT5-Flag in 293T cell lysates. 293T cells were treated with AR-MeTAG **1** (5 μmol/L) for 24 h. The antagonistic effect of PRMT5 inhibitor was measured by pretreating with GSK3326595 (20 μmol/L), followed by treatment with AR-MeTAG **1** (5 μmol/L) for 24 h. WCL, whole cell lysate. (F) AR-MeTAG **1** induced SDMA modification on AR. 293T cells were transfected with PRMT5-Flag and AR-HA, and subsequently treated with or without AR-MeTAG **1** (5 μmol/L) for 24 h. Cell lysates were harvested to detect SDMA modification by Co-IP and Western blot analysis. (G) AR-MeTAG **1** introduced SDMA on AR in a PRMT5-dependent manner. VCaP cells were depleted with PRMT5 using shRNA, and then treated with AR-MeTAG **1** (5 μmol/L) for 24 h, followed by Co-IP and Western blot analysis.

treatment, evaluation of the combination index suggested no synergic effect between GSK3326595 and enzalutamide (Fig. S1I). In addition, AR-MeTAG **1** reduced the anchorage-independent growth of C4-2 cells in the colony formation assay, which was more effective than GSK3326595 and enzalutamide (Fig. 4B and C). Furthermore, AR-MeTAG **1** induced a dose-dependent apoptosis, which was slightly more effective than GSK3326595 and enzalutamide (Fig. 4D and E). Consistently, AR-MeTAG **1** treatment caused a subtle decrease in total PARP protein level, and in turn a slight increase in cleaved PARP protein level (Fig. S1J). To further verify that AR-MeTAG **1** induces apoptosis in C4-2 cells through AR methylation, we constructed the AR-R761K mutant, which prevents AR methylation. The mutation of amino acid R761 in AR to K rendered AR-MeTAG **1** incapable of inducing apoptosis in C4-2 cells, further confirming that AR-MeTAG **1** promotes apoptosis by inducing methylation of

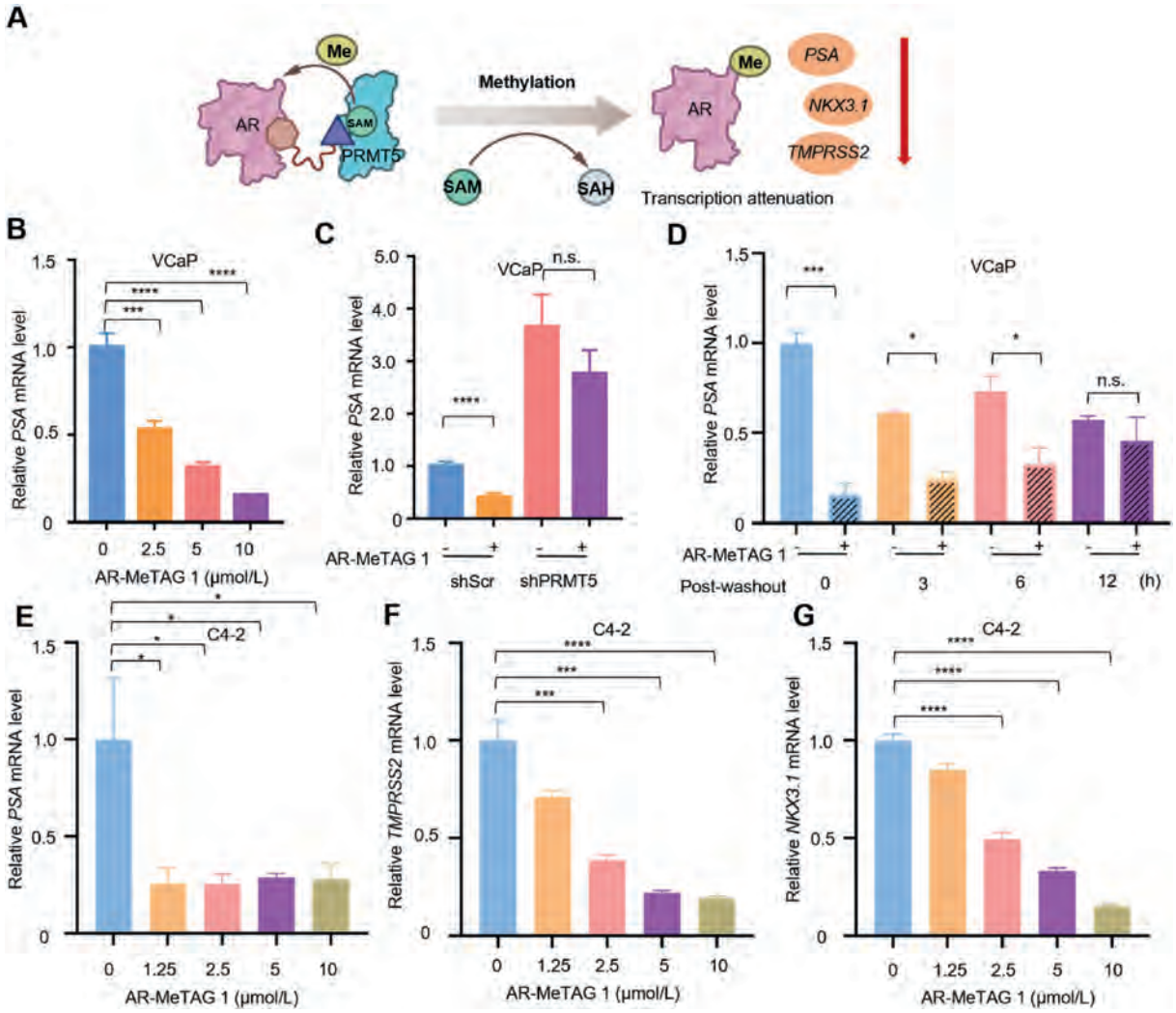

Figure 3 AR-MeTAG **1** attenuates AR's transcriptional function. (A) Schematic diagram showing the decrease in transcription of AR target genes, *PSA*, *NKX3.1* and *TMPRSS2*, induced by AR-MeTAG **1**. (B) AR-MeTAG **1** downregulated the *PSA* mRNA levels in a concentration-dependent manner. VCaP cells were treated with AR-MeTAG **1** for 24 h, as monitored by RT-qPCR. (C) The reduction in *PSA* mRNA levels induced by AR-MeTAG **1** was dependent on PRMT5. *PSA* mRNA levels were detected by RT-qPCR after VCaP cells being treated with AR-MeTAG **1** (10 μmol/L) for 24 h with or without knockdown of endogenous *PRMT5*. (D) Washout experiments showed increased *PSA* mRNA level upon removal of AR-MeTAG **1** from VCaP cells. VCaP cells were pretreated with AR-MeTAG **1** (10 μmol/L) or vehicle for 12 h, washed with PBS, and cultured in fresh media (without AR-MeTAG **1**) for the indicated time. (E−G) Treatment with AR-MeTAG **1** caused down-regulation of *PSA* (E), *TMPRSS2* (F) and *NKX3.1* (G) mRNA levels in C4-2 cells in a dose-dependent manner. C4-2 cells were treated with indicated concentrations of AR-MeTAG **1** for 24 h. Nonparametric Brown−Forsythe test ($n = 3$), mean ± SD, n.s. not significant, $^{*}P < 0.05$; $^{***}P < 0.001$; $^{****}P < 0.0001$.

AR (Fig. S1K and S1L). Since PSA has been reported to enhance AR transactivation by modulating the p53 pathway, resulting in reduced apoptosis and increased cell proliferation in prostate cancer cells, we hypothesized that the pro-apoptotic effect of AR-MeTAG **1** may be linked to its ability to suppress AR transcriptional activity. This suppression likely leads to the downregulation of PSA, which subsequently induces cell apoptosis. Moreover, AR-MeTAG **1** showed the ability to inhibit C4-2 cell migration, in contrast to GSK3326595 and enzalutamide (Fig. 4F and G). Taken together, AR-MeTAG **1** recruits endogenous PRMT5 to methylate and inhibit AR, thus possesses the potential to suppress the proliferation of prostate cancer cells, possessing the potential as a hit compound to be further developed for prostate cancer treatment through PRMT5-mediated AR inhibition.

*2.3. AKT-MeTAG **1** mediates PRMT5−AKT interaction and facilitates arginine methylation of AKT*

To assess whether chemically induced arginine methylation system could be extended to other target proteins, we further developed heterobifunctional molecules to manipulate AKT methylation. Through loss of function assays, such as PRMT5 depletion or R-to-K mutation of the substrate, AKT has recently been found as an arginine methylation substrate of PRMT5, and this methylation leads to AKT activation[36,37]. However, there is still a lack of available tools to specifically manipulate the arginine methylation of AKT in cells without disturbing other PRMT5 substrates. Thus, we used a pan-AKT ligand AZD5363[48] which has been advanced into clinical trials for solid tumors for AKT-

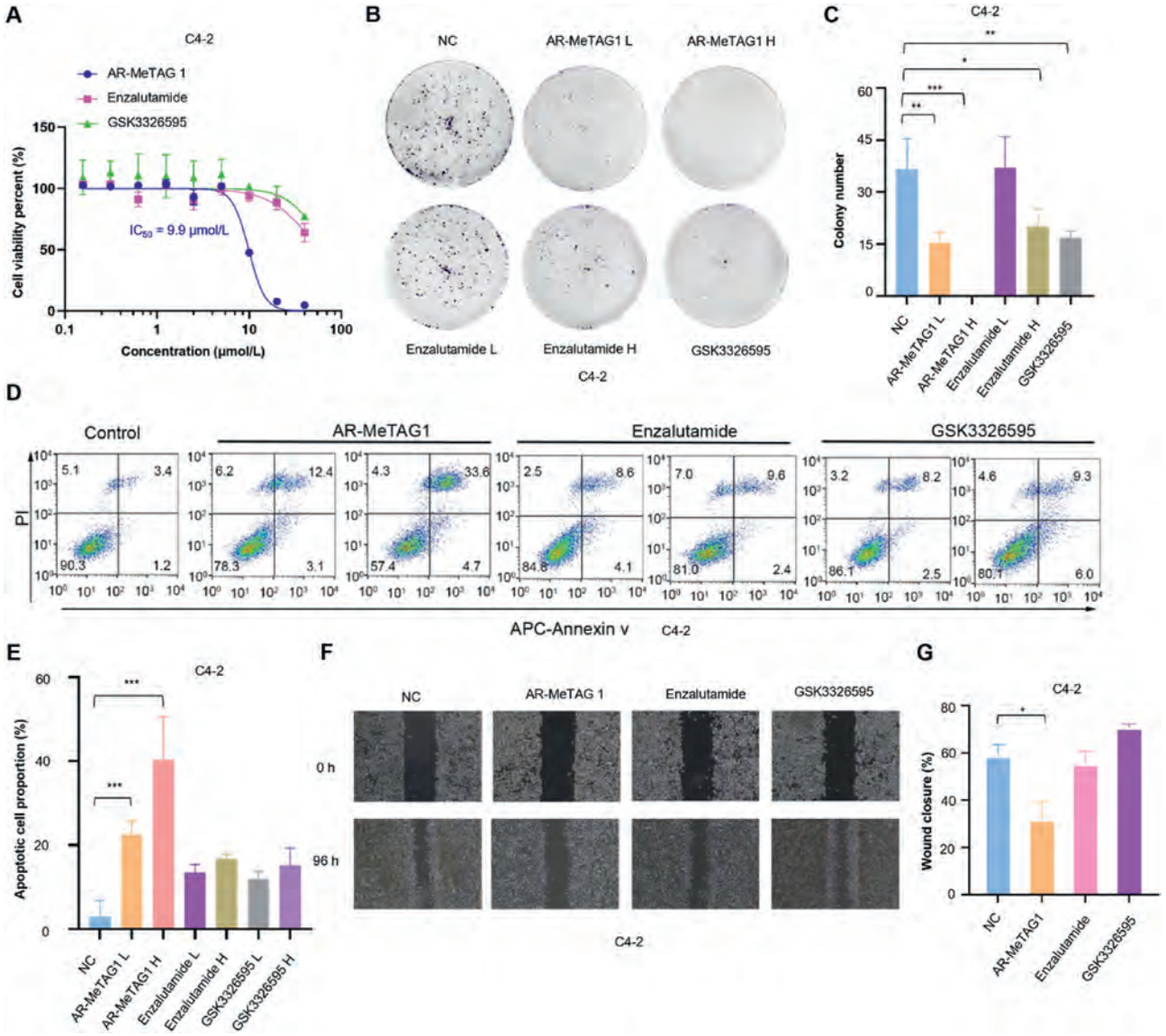

Figure 4 AR-MeTAG **1** inhibits the proliferation of prostate cancer cells. (A) AR-MeTAG **1** was able to suppress the proliferation of C4-2 cells. Cell viability of C4-2 cells was detected after 48 h of treatment with AR-MeTAG **1**, enzalutamide, and GSK3326595. (B, C) Representative images (B) and the statistical results (C) showed that AR-MeTAG **1** inhibited the colony formation ability of C4-2 cells. Cells were treated with AR-MeTAG **1** (L: 5 μmol/L, H: 10 μmol/L), enzalutamide (L: 5 μmol/L, H: 10 μmol/L) and GSK3326595 (10 μmol/L) for 7 days, $n = 3$. (D) AR-MeTAG **1** could induce apoptosis of C4-2 cells. The apoptosis was assessed by flow cytometry after C4-2 cells being treated with AR-MeTAG **1** (L: 5 μmol/L, H: 10 μmol/L), enzalutamide (L: 5 μmol/L, H: 10 μmol/L) and GSK3326595 (L: 5 μmol/L, H: 10 μmol/L) for 24 h. (E) Statistical analysis of three independent apoptosis detection, $n = 3$. (F, G) Representative images (F) and the statistical results (G) showed that AR-MeTAG **1** inhibited the migration ability of C4-2 cells. Cells were treated with AR-MeTAG **1** (5 μmol/L), enzalutamide (5 μmol/L) and GSK3326595 (5 μmol/L). One-way ANOVA analysis ($n = 3$), mean ± SD, $^{*}P < 0.05$; $^{**}P < 0.01$; $^{***}P < 0.001$.

MeTAG design. Analysis of the co−crystal structure of AKT in complex with AZD5363 indicated that the hydroxyl group is solvent-exposure and thus being an attachment point. Based on previous structure−activity relationship (SAR) studies, the hydroxyl group was replaced by a piperazine ring[49] to hinge with PRMT5 ligand (**3**) *via* various linkers, yielding AKT-MeTAG **1**−**3** (Fig. 5A, Supporting Information Fig. S3A and Supporting Information Scheme S2).

First, docking studies were performed to predict the SAR. Docking indicated that AKT-MeTAG **1** adopted a U conformation with its warheads binding with AKT and PRMT5 respectively to form a stable ternary complex (Fig. 5B and C). In comparison, both AKT-MeTAG **2** and **3** are more compact and only bind to PRMT5 (Supporting Information Fig. S4). Next, *in vitro* FP assay demonstrated the AKT: AKT-MeTAG **1**: PRMT5 complex formation facilitated by AKT-MeTAG **1** with a median concentration of 311 nmol/L, while other compounds could not (Fig. 5D). In line with these results, a continuous increase in fluorescence polarization value was observed only for AKT-MeTAG **1** after successive addition of AKT and PRMT5 proteins (Fig. S3B). In contrast, the fluorescence polarization value remained unchanged for AKT-MeTAG **2** and **3** with the increased concentration of PRMT5

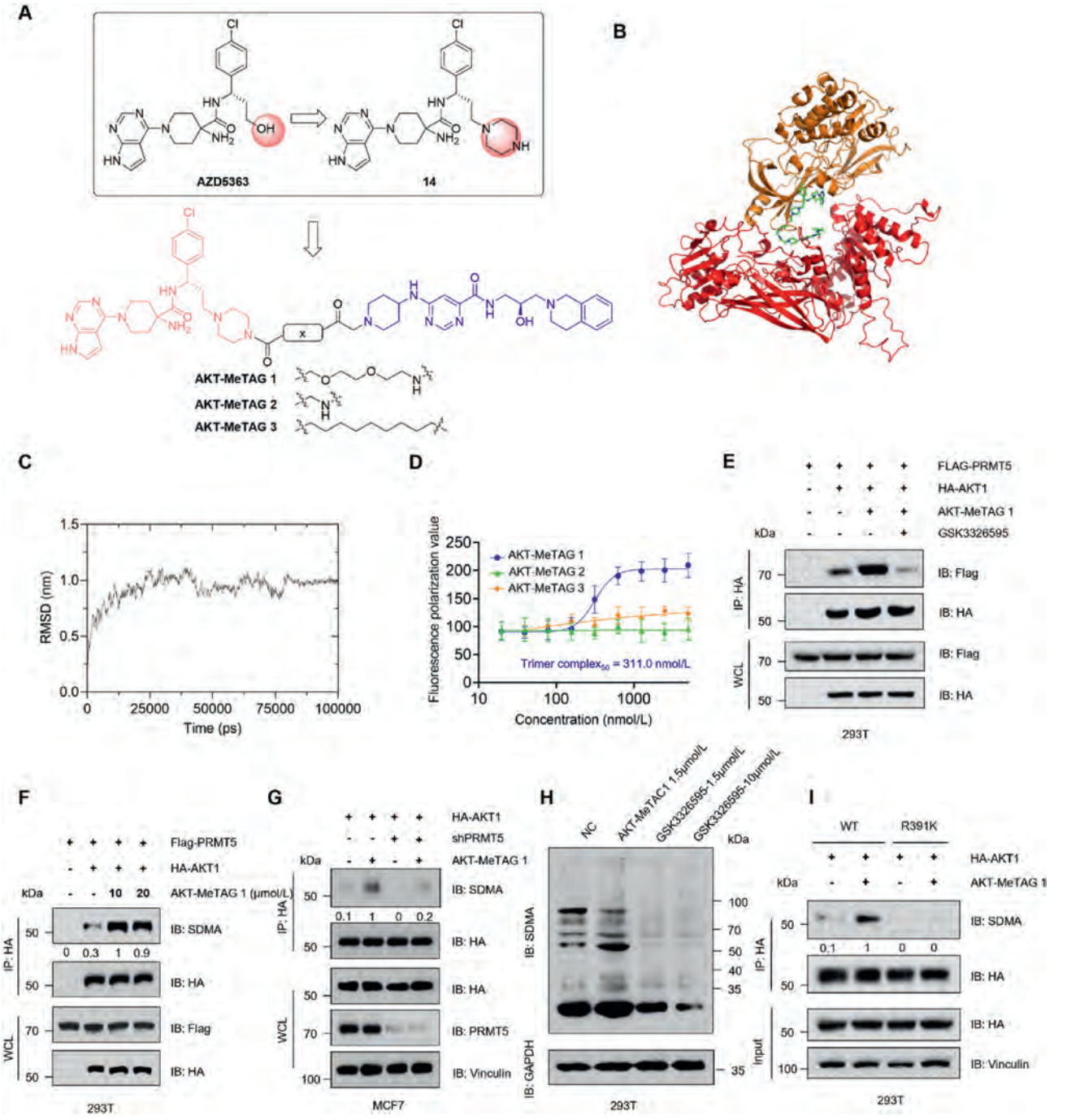

Figure 5 Development of AKT-MeTAG. (A) Schematic overview of the AKT-MeTAG system. (B) The predicted binding mode of the AKT: AKT-MeTAG **1**: PRMT5 ternary complex (orange: AKT, red: PRMT5). (C) The RMSD curve of the ternary complex. (D) AKT-MeTAG molecules induced ternary complex formation detected by FP assay. (E) Co-IP analysis of 293T cell lysates showed the ternary complex formation induced by AKT-MeTAG **1** (1.5 μmol/L, 24 h), which can be antagonized by excessive GSK3326595 (20 μmol/L). (F) AKT-MeTAG **1** (10/20 μmol/L, 24 h) induced SDMA of AKT. (G) AKT-MeTAG **1** induced SDMA of AKT in a PRMT5-dependent manner. MCF7 cells were infected with lentivirus to knock down endogenous *PRMT5*, and then treated with AKT-MeTAG **1** (1.5 μmol/L) for 24 h. (H) Immunoblot analysis of global methylation in 293T cells treated with DMSO, AKT-MeTAG **1** (1.5 μmol/L) and GSK3326595 (1.5 or 10 μmol/L). (I) AKT-MeTAG **1** induced SDMA of AKT on the R391 residue. MCF7 cells stably expressing AKT1-WT or R391K were treated with AKT-MeTAG **1** (1.5 μmol/L, 24 h).

protein. These data suggest that only AKT-MeTAG **1** was able to include ternary complex formation. AKT-MeTAG **1**-induced interaction between PRMT5 and AKT was further validated through the co-immunoprecipitation (Co-IP) in 293T cells transfected with PRMT5 and AKT1, and this effect could be disrupted by PRMT5 inhibitor GSK3326595 (Fig. 5E). Consequently, AKT-MeTAG **1** augmented arginine methylation of AKT, while AKT-METAG **2** and **3** could not (Fig. 5F, Fig. S3C and

S3D), and depletion of *PRMT5* largely hindered the effect in MCF7 cells (Fig. 5G). Considering that the ligand of PRMT5 in MeTAG was derived from its inhibitor, which might exhibit inhibitory effects against PRMT5, we further analyzed the overall arginine methylation level after MeTAG treatment. Unlike GSK3326595, AKT-MeTAG **1**, at the concentration used in this study, did not cause alterations in global arginine methylation (Fig. 5H), suggesting that in MeTAG, the warhead of PRMT5 had a weak effect in inhibiting PRMT5. Since R391 has been reported as a major site in AKT1 that could be methylated by PRMT5 at physiological condition[36], we further showed that AKT-MeTAG **1** induced SDMA on wild type AKT but not the R391K mutation (Fig. 5I), indicating that AKT-MeTAG **1** induced SDMA of AKT on the same R391 residue. Though AKT is also a PTM enzyme, no cross-talk of methylation and phosphorylation was observed with AKT-MeTAG **1** treatment as the pPRMT5 level remained unchanged (Fig. S3E).

2.4. PRMT5-mediated AKT methylation promotes its activation

Robust evidences have proved the involvement of PRMT5-mediated arginine methylation in the activation of the AKT signaling pathway, and impaired AKT phosphorylation and activation has been observed consequent to *PRMT5* depletion[36,37,50,51]. Thus, we further investigated the effects of AKT-MeTAG **1** in regulating AKT phosphorylation in cells. Upon treatment with AKT-MeTAG **1**, there was a significant dose- and time-dependent elevation in the levels of AKT-pT308 and AKT-pS473 in both 293T and MCF7 cells (Fig. 6A and B), compared to AKT-MeTAG **2** (Fig. S3F). Given that the warhead of AKT (AZD5363) used in this study was reported to increase the level of AKT pT308 and pS473[48], a control compound for AKT-MeTAG series, termed as AKT-MeTAG Control (AKT-MeTAG Ctr, Fig. S3A), was synthesized to distinguish whether the increased AKT pT308 and pS473 level is totally induced by MeTAG or not. AKT-MeTAG Ctr bears the AKT binding warhead while lacks PRMT5 binder and thus fails to recruit PRMT5 to AKT for SDMA. As shown in Fig. S3G, AKT-MeTAG Ctr elevated AKT pT308 and pS473 levels, with weaker effect than AKT-MeTAG **1**, indicating that the increase of AKT pT308 and pS473 levels by AKT-MeTAG **1** might be comprised of AKT inhibition and recruitment of PRMT5 for SDMA. Moreover, both competitive inhibition of PRMT5 by GSK3326595 and genetic knockdown of *PRMT5* using shRNA significantly blocked the effect of AKT-MeTAG **1** in elevating AKT phosphorylation level (Fig. 6C and D). Additionally, upon removal of AKT-MeTAG **1** from cells, AKT phosphorylation gradually returned to basal level (Fig. 6E). These findings collectively suggest that AKT-MeTAG **1** acts as a reversible positive regulator for AKT activation, through recruiting PRMT5 to methylate AKT on its R391 residue.

Besides, a recent study has shown that transient PI3K activation can promote cell proliferation and neurite outgrowth, providing cardio protection from ischemia-reperfusion injury and enhancing nerve regeneration following nerve crush[52]. Thus, short-term activation of PI3K−AKT signaling pathway has the potential for tissue protection and regeneration. To this end, AKT-MeTAG **1** was tested for its ability to promote cell growth. In line with the upregulated kinase activity of AKT mediated by AKT-MeTAG **1** induced arginine methylation, H9C2, HDF, HUVEC and MCF7 cells displayed increasing cell proliferation with AKT-MeTAG **1** treatment, compared to that with DMSO, GSK3326595 and AZD5363 treatment (Fig. 6F−K and Fig. S3H and S3I). However, at this stage, it is challenging to determine whether AKT-MeTAG **1** promotes cell growth, as its proliferation effect appears moderate compared to the control. Further chemical and biological studies are required to confirm whether AKT-MeTAG **1** enhances cell growth through AKT methylation.

2.5. MeTAG-mediated arginine methylation on a neo-substrate protein p300

Encouraged by the satisfied results observed for MeTAGs of AKT and AR in causing proximity-induced arginine methylation, we next extend to investigate methylation on proteins not being reported as substrates of PRMT5. Given the important transcriptional co-activator role of p300 in myriad cellular processes[53,54], we sought to investigate whether p300 could be methylated by its MeTAG. Utilizing the p300 bromodomain (BRD) ligand[55], a series of bifunctional molecules consisting different types of linkers were achieved (Fig. 7A, Supporting Information Fig. S5A and Supporting Information Scheme S3). The designed heterobifunctional small molecules were first docked into the enzymes. Docking analysis indicated that p300-MeTAG **1** was superior to the rest compounds in inducing the formation of a stable p300: p300-MeTAG: PRMT5 complex, as it bridged p300 and PRMT5 with its two warheads (Fig. 7B and C and Supporting Information Fig. S6). Subsequently, these molecules were assayed for their ability to induce trimer complex formation between PRMT5 and the BRD domain of p300 *in vitro*. As shown in Fig. 7D, p300-MeTAG **1** exhibited potential for trimer complex formation, as measured by FP assay, while p300-MeTAG **2** showed lower efficiency. Consistently, the fluorescence polarization value keeps rising with increased concentration of p300 and PRMT5 protein for p300-MeTAG **1**, in contrast to that for p300-MeTAG **2/3/4**, confirming the ability of p300-MeTAG **1** rather than p300-MeTAG **2/3/4** for mediating the trimer complex formation (Fig. S5B). Thus, p300-MeTAG **1** was selected for further investigation. Consistent with its binding affinity, p300-MeTAG **1** facilitated complex formation between p300 and PRMT5, initiating a proximity-induced methyl transfer process that robustly increased the arginine methylation level of p300 (Fig. 7E). As p300 has not been reported as a PRMT5 substrate, we further explored potential arginine methylation sites on p300 mediated by PRMT5 using mass spectrometry (MS) analysis with or without p300-MeTAG **1** treatment. The MS analysis revealed that p300 had basal arginine methylation at the R237, R695 and R2059 residues, while p300-MeTAG **1** treatment led to methylation at 12 additional arginine sites (Fig. S5D). Moreover, MeTAG-mediated p300 modification was effectively antagonized by depletion of endogenous *PRMT5* (Fig. 7F), indicating it functioned in a PRMT5-dependent manner. Similar to AKT-MeTAG, p300-MeTAG **1** only increased the methylation level of POI without affecting the PRMT5Ac level (Fig. S5C). These results substantiate the capability of p300-MeTAG **1** to induce arginine methylation on p300, providing a research tool for studying protein arginine methylation for any POIs.

Considering the important transcriptional co-activator role of p300 in cells and the unknown function of p300 arginine methylation, we set out to investigate the downstream pathways of methylated p300. Since p300 plays a prominent role in rapid genetic responses, and it will induce rapid expression of many classic primary response genes, including *FOS* and *EGR2*[56], we evaluated the levels of these two genes after p300-MeTAG **1** treatment. As shown in Fig. 7G and H, p300-MeTAG **1**

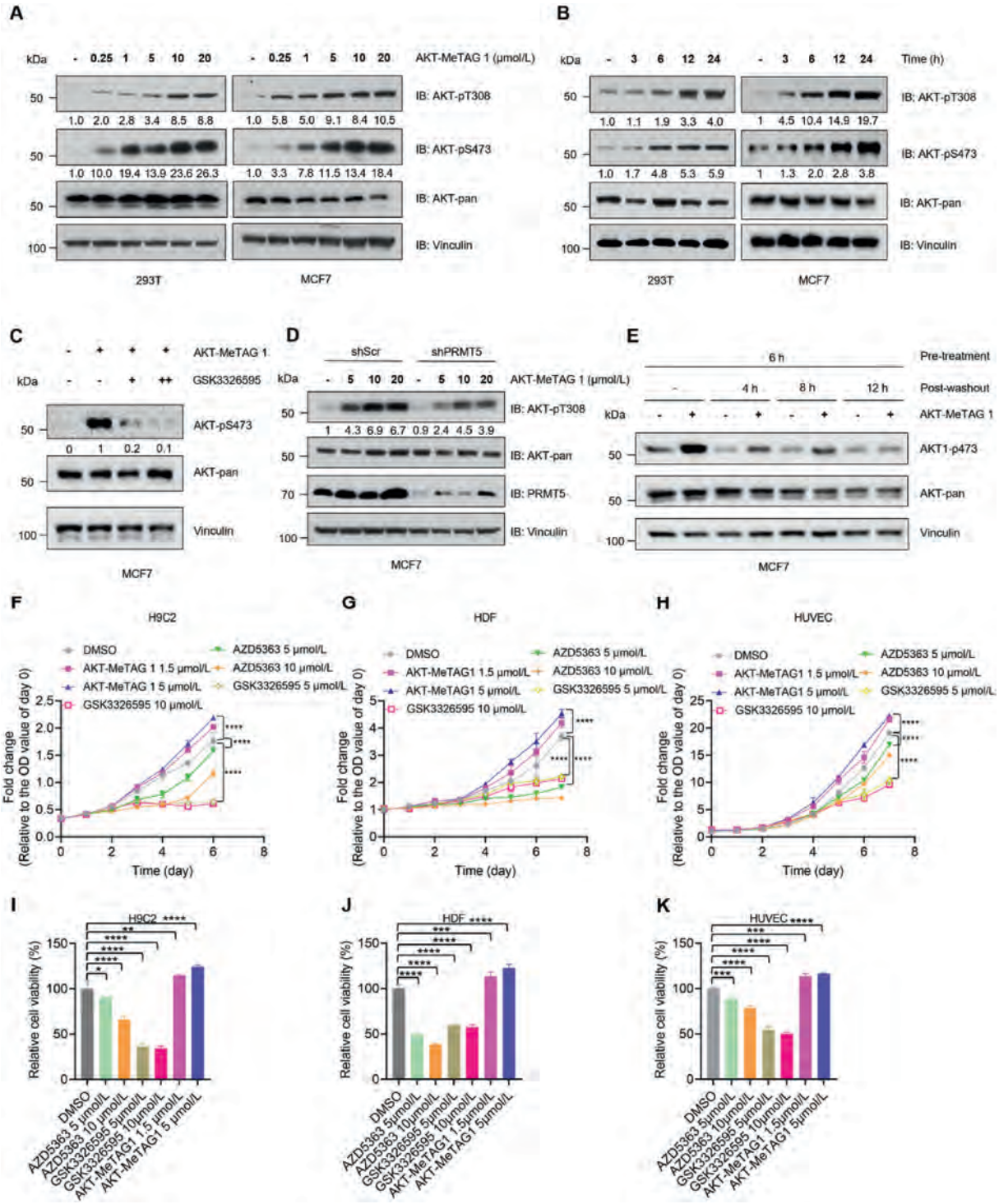

Figure 6 AKT-MeTAG activates AKT. (A) AKT-MeTAG **1** activated AKT1 in a dose-dependent manner. MCF7 cells were treated with indicated concentrations of AKT-MeTAG **1** for 24 h, followed by immunoblot analysis of AKT-pT308/pS473. (B) AKT-MeTAG **1** activated AKT1 in a time-dependent manner. MCF7 cells were treated with AKT-MeTAG **1** (1.5 μmol/L) for indicated hours, followed by immunoblot analysis of AKT-pT308/pS473. (C) AKT-MeTAG **1** activated AKT1 in a PRMT5 activity-dependent manner. MCF7 cells were treated with AKT-MeTAG **1** (1.5 μmol/L) with or without GSK3326595 (+, 5 μmol/L; ++, 50 μmol/L) for 24 h. (D) AKT-MeTAG **1** activated AKT1 in a PRMT5-dependent manner. MCF7 cells were knocked down of *PRMT5*, and treated with AKT-MeTAG **1** for 24 h. (E) The phosphorylation of AKT1 is reversible. MCF7 cells were pretreated with AKT-MeTAG **1** (1.5 μmol/L) or vehicle for 6 h, washed with PBS, and cultured in fresh media (without AKT-MeTAG **1**) for the indicated hours. (F−H) AKT-MeTAG **1** promoted H9C2 (F), HDF (G) and HUVEC (H) cell growth. Two-way ANOVA analysis ($n = 3$), mean ± SD, ****$P < 0.0001$. (I−K) H9C2 (I), HDF (J) and HUVEC (K) cell viability on last day in curve F−H. One-way ANOVA analysis ($n = 3$), mean ± SD, *$P < 0.05$, **$P < 0.01$, ***$P < 0.001$, ****$P < 0.0001$.

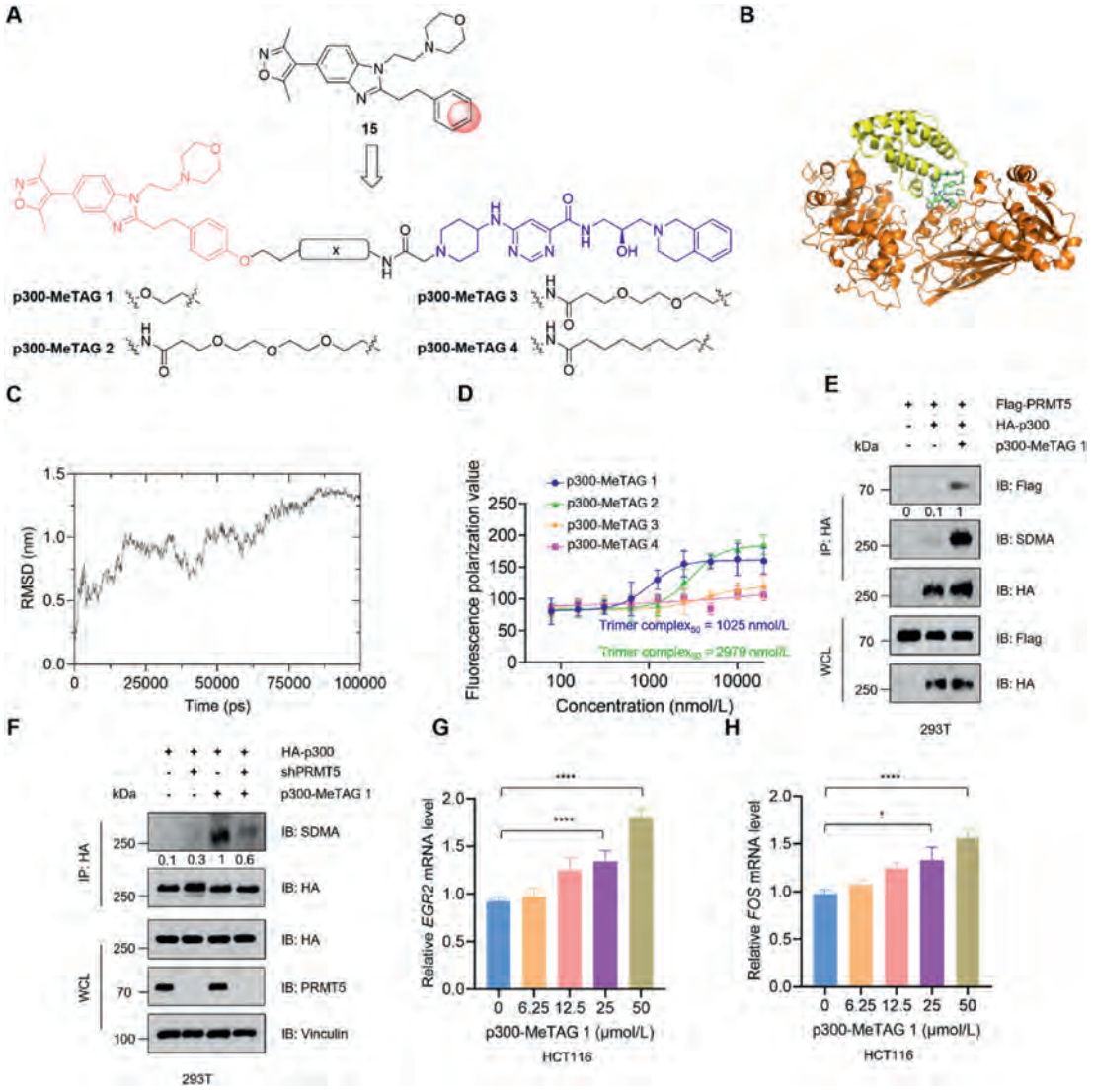

Figure 7 Development of p300-MeTAG for arginine methylation of p300. (A) Schematic overview of the p300-MeTAG system. (B) The predicted binding mode of the p300: p300-MeTAG **1**: PRMT5 ternary complex (yellow: p300, orange: PRMT5). (C) The RMSD curve of the ternary complex. (D) p300-MeTAG molecules induced ternary complex formation in FP assay. (E) Co-IP of p300-HA and PRMT5-Flag in 293T cell lysates showed the ternary complex formation and p300 arginine SDMA mediated by p300-MeTAG **1** (20 μmol/L, 24 h). (F) P300-MeTAG **1** induced SDMA of p300 in a PRMT5-dependent manner. Co-IP analysis of 293T cells with or without knockdown of endogenous *PRMT5* being treated with p300-MeTAG **1** (20 μmol/L) for 24 h for p300 arginine SDMA. (G) p300-MeTAG **1** upregulated the *EGR2* mRNA levels in a concentration-dependent manner. HCT116 cells were treated with p300-MeTAG **1** for 24 h, as monitored by RT-qPCR. (H) p300-MeTAG **1** upregulated the *FOS* mRNA levels in a concentration-dependent manner. HCT116 cells were treated with p300-MeTAG **1** for 24 h, as monitored by RT-qPCR. Nonparametric Brown−Forsythe test ($n = 3$), mean ± SD, $^{*}P < 0.05$; $^{****}P < 0.0001$.

upregulated the *FOS* and *EGR2* mRNA levels in HCT116 cells, which was in accordance with the literature reported observation, suggesting the possibility of p300-MeTAG **1** mediated p300 activation. The uncropped immunoblots are shown in Supporting Information Figs. S7−S11.

3. Conclusions

Arginine methylation is a critical post-translational modification involved in the regulation of protein function. Targeted modulation of arginine methylation on specific proteins enables precise control over particular aspects of protein activity, which is essential for various cellular processes. Recent advancements in heterobifunctional small molecules such as PROTAC[57], DUBTAC[30], PHICS[31,58], PHOTAC[32,59], AceTAG[33], OGT/β-catenin dual-specificity aptamers[34], OGTAC[35], and MrTAC[60] have demonstrated significant potential for modulating the post-translational modifications of target proteins. These molecules facilitate the targeted control of modifications like ubiquitination, deubiquitination, phosphorylation/dephosphorylation, acetylation, *o*-GlcNAcylation and methylation. Inspired by the success of these bifunctional molecules, which possess several favorable attributes including ease of synthesis and standardization, genomic non-integration, and low immunogenicity, we have developed a novel methylation tagging system termed MeTAG. This system combines a PRMT5 ligand with a POI ligand to enable efficient

and selective modulation of arginine methylation on specific target proteins.

We have developed compounds that target and regulate arginine methylation in a PRMT5-dependent manner for three key proteins: AR, p300, and AKT. These compounds have successfully enabled precise control over arginine methylation for each of these targets. Specifically, AR-MeTAG **1** facilitates the methylation-dependent inhibition and modulation of AR function, while AKT-MeTAG **1**-mediated arginine methylation of AKT enhances its activity and promotes cell proliferation. These findings demonstrate the efficacy of the MeTAG strategy in fine-tuning protein function through targeted arginine methylation. Additionally, by applying p300-MeTAG **1**, we identified novel methylation sites on the p300 protein, underscoring MeTAG's utility not only as a therapeutic intervention but also as a research tool for mapping previously unknown methylation sites. This approach establishes MeTAG as a versatile strategy for both functional regulation and detailed characterization of amino acid methylation in target proteins.

In this study, MeTAG using PRMT5 inhibitor as its ligand effectively induces methylation in POIs. We hypothesize that the observed blunted effect on PRMT5 inhibition with MeTAG might be due to that the warhead towards PRMT5 is derived from its inhibitor GSK3326595, which is uncompetitive with SAM but competitive with the peptide substrate. When the MeTAG brings a POI close to PRMT5, the sidechain of protein bearing arginine residue to be methylated is also close to the pocket where GSK3326595 occupies, and thus dynamically competing with GSK3326595 and weakening the inhibitory effect of MeTAG on PRMT5. In addition, the naturally occurring recognition of endogenous substrates by PRMT5 (*e.g.* AR, AKT and p300) might impart positive cooperativity, contributing to the delayed auto-inhibition, as observed in other heterobifunctional systems[33,61,62]. Moreover, we briefly investigated the effect of linker on the efficiency of MeTAG system. Both linker length and type will affect the formation of the ternary complex and subsequent methylation, indicating the linker preference of the POI. Our simulations also reveal that if the linker is too short or its structural properties hinder trimer formation, the second protein is unable to establish a stable complex with the bifunctional molecule and the first protein. Conversely, when the linker is excessively long, a trimeric structure is observed; however, detailed structural analysis indicates that the spatial separation between proteins prevents meaningful interactions. Furthermore, the function of MeTAG is dependent on the biological function of the POI methylation and is unrelated to the ligand used in the MeTAG, as exemplified in AR-MeTAG and AKT-MeTAG.

Overall, we provide a generalizable MeTAG approach to manipulate the arginine methylation of POIs, which serves as a useful chemical tool for understanding the biological function of protein methylation with potential translational value. More importantly, our findings demonstrate the potential of MeTAG for therapeutic benefit, through accurately manipulating the methylation state of a specific POI.

4. Experimental

4.1. Cell culture and transfection

The cell lines used in this study were purchased from American Type Culture Collection (ATCC; Manassas, VA, USA). HEK293T, H9C2, HDF and MCF7 cell lines were cultured in Dulbecco's modified Eagle's medium (DMEM) supplemented with 10% fetal bovine serum (FBS, BI, USA), 100 U/mL penicillin and 0.1 mg/mL streptomycin (Gibco; ThermoFisher Scientific, Rochester, USA). VCaP and HUVEC cell lines were cultured in RPMI-1640 medium containing 10% FBS. All cells were maintained at 37 °C and 5% CO_2. For transfection, lipofectamine 2000 transfection reagent purchased from Life Technologies was used according to the manufacturer's protocol. Various cell lines were infected with lentiviral and retroviral cDNA expressing viruses, which were packaged in HEK293T cells. The lentiviral vector loaded with *PRMT5* shRNA was transfected into indicated cells.

4.2. Antibodies, reagents, and plasmids

Antibodies SDMA (13222), PRMT5 (2252), AKT-pT308 (13038), AKT-pS473 (4060), AKT-pan (4685), Flag-tag (14793), HA-tag (3724), PARP (9532), Acetylated-Lysine (9441S), Vinculin (4650) were purchased from Cell Signaling Technology. Secondary anti-rabbit antibody and secondary anti-mouse antibody were purchased from Sigma−Aldrich. pcDNA3.1-HA AKT1 (78778) was purchased from Addgene. pcDNA3.1-Flag-PRMT5 (OHu23684) was purchased from GenScript. AR and p300 cDNA were amplified and cloned into the pcDNA3-HA vector. HA-AR R761K mutant was generated by site mutagenesis using QuickChange Lightning Site-Directed Mutagenesis Kit (Agilent). Agilent PrimerDesign Program was used to design primers for introducing mutation sites. HA AR-R761K (forward 5′-aGATGCTC-TACTTCGCCCCTGATCTGG-3′, reverse primer 5′-TGGAGTT-GACATTGGTGAAGGATCGC-3′). Oligonucleotide sequences for shRNA targeting *PRMT5* were as follows: *shPRMT5*-1 (5′-GCCCAGTTTGAGATGCCTTAT-3′), *shPRMT5*-2 (5′-CCCA TCCTCTTCCCTATTAAG-3′).

4.3. Protein expression

The proteins investigated in this study were acquired through bacterial expression. Based on the ligand binding information associated with the target proteins, we expressed the full-length PRMT5, AR ligand binding domain, p300 bromodomain, and AKT kinase domain, respectively. To enhance protein solubility and facilitate subsequent purification, a GST tag was added to PRMT5, while AR, p300, and AKT proteins were tagged with His. The pGEX-5x-1 plasmid served as the expression vector. Plasmid synthesis and protein expression were conducted by General Bio.

4.4. Fluorescence polarization

Fluorescence polarization (FP) experiments were conducted in Microfluor 384 black well plates (ThermoFisher Scientific, Rochester, USA) utilizing a Tecan Ultra plate reader. The objective was to assess the ability of MeTAG to induce trimer complex formation involving the protein of interest and PRMT5. To achieve this, PRMT5 was initially labelled with Cy3.

In the experimental procedure, a one-to-one concentration mixture of the protein of interest and MeTAG was incubated for 20 min. The mixture, ranging from 5 μmol/L to 20 nmol/L, was then used for trimer incubation. Subsequently, 100 nmol/L Cy3-labeled PRMT5 was introduced into the wells and incubated for an additional 20 min. FP values were measured using the Tecan Ultra

plate reader. During analysis, PBS served as the background, and Cy3-labeled PRMT5 alone was utilized as the control.

4.5. Cell-based PRMT5 inhibition assay

C4-2 cells were plated at a density of 4×10^3 per well on 96-well plates. Indicated drugs were twofold serially diluted in duplicate in the medium of choice, and an equal volume (100 μL) of serial drug dilution was added to the plates with cells (100 μL/well). Plates were incubated at 37 °C for 24 h. Medium was harvested and assayed using enzyme linked immunosorbent assay (ELISA). Briefly, to the plate immobilized with PRMT5 antibody was added the sample solution, followed by incubation with HRP tagged detection antibody at 37 °C for 1 h. Then, 3,3′,5,5′-tetramethylbenzidine (TMB) was used as the detection system (450 nm).

4.6. Molecular docking

Molecular docking is a method for predicting the preferred orientation of a molecule (ligand) when it binds to another molecule (receptor, such as a protein or enzyme). In this study, we employed a semi-flexible docking approach to form stable complexes. To predict plausible ternary complexes, we divided the small molecule into three parts: the two ligand parts that bind with the target protein and PRMT5 and the linker part. We docked the ligand part with the corresponding target protein, and then constructed the binding conformations of two proteins with the small molecule based on the docking site or the active region of the protein.

Firstly, we downloaded the crystal structure of the target protein from the Protein Data Bank (www.rcsb.org). Subsequently, we prepared the protein using the AutoDock 1.5.2 software. During the preparation process, we removed water molecules, added polar hydrogen atoms, and calculated Gasteiger charges. We then performed a local charge distribution on the protein and defined the AutoDock atom types. To understand the torsion angles and rotatable bonds of the molecule, we utilized the Torsion Tree menu in ADT for viewing and specification. Secondly, we set parameters in the Grid module. We defined the box size of the docking area as $40 \times 40 \times 40$ grid box size (Å) to encompass the entire active site of the protein molecule. Other parameters were kept at their default values. For the small molecule, we prepared it using the AutoDock software. Molecular docking was performed using the AutoDock Vina software. Finally, we constructed the initial model of the ternary complex using the Discover Studio software to build the active site of the reference protein and the docking results.

4.7. Molecular dynamics simulation

To further investigate the interactions and stability of the ternary complex, this study employed molecular dynamics simulation (MD) technology, using the GROMACS 2021 software to simulate a 100-ns ternary complex. The AMBER99SB-ILDN force field was selected to establish the protein topology file, and the small molecule ligand topology file was generated using the sobtop software and the GAFF force field. A truncated cubic TIP3P solvent box was added at a distance of 1 nm from the system, and Na/Cl was added to the system to balance the charge. Then, energy minimization was performed using 2500 steps of the steepest descent method and 2500 steps of the conjugate gradient method. Under the condition of maintaining the system temperature at 298.15 K, a 100-ps NVT ensemble simulation and a 100-ps NPT equilibrium simulation were conducted. Finally, under periodic boundary conditions, a 30-ns or 50-ns dynamic simulation was performed, with long-range electrostatic interactions calculated using the PME method, a non-bonded cutoff distance set at 1 nm, the system pressure at 101.325 kPa, an integration time step of 2 fs, and trajectory saved every 100 ps.

Through molecular dynamics simulation, the binding conformations between the two proteins and the molecule were obtained, allowing for a deeper understanding of the interaction mechanisms. At the same time, by extracting stable molecular conformations from the equilibrium trajectory, the role of the small molecule in forming the complex structure can be further understood by observing the interactions formed between the molecule and the proteins.

4.8. Immunoprecipitation assay and immunoblot analysis

Briefly, cells were lysed with EBC lysis buffer [50 mmol/L of Tris−HCl (pH 7.4), 120 mmol/L of NaCl, 5 mmol/L of EDTA, 0.5% of NP-40] containing protease inhibitors (Sigma−Aldrich; Merck KGaA, MO, USA) and phosphatase inhibitors (Sigma−Aldrich; Merck KGaA, MO, USA). The proteins were incubated with the monoclonal anti-FLAG (A2220, Sigma−Aldrich, MO, USA) or anti-HA (A2095, Sigma−Aldrich, MO, USA) antibody-conjugated M2 agarose beads with gentle rocking at 4 °C for 4 h. Subsequently, cell lysates were washed with EBC buffer and the proteins were extracted from the beads by boiling at 95 °C for 5 min. For immunoprecipitation assays, the proteins were separated by sodium dodecyl sulfate-polyacrylamide gel electrophoresis (SDS-PAGE) gels. Then they were transferred to polyvinylidene fluoride (PVDF) membranes and incubated with specific primary antibodies at 4 °C overnight. After incubating with HRP-conjugated secondary antibody for 1 h at room temperature, the protein immunoreactive signals were tested by ECL detection system (ThermoFisher Scientific, Rochester, USA) or ECL chemiluminescence system (Santa Cruz Biotechnology, TX, USA). All the immunoblotting assays were repeated at least three times with similar results. For semi-quantitative analysis, immunoblot bands were analyzed using ImageJ software (NIH).

4.9. Cell viability tests by cell counting Kit-8 (CCK-8)

To evaluate the cell viability, C4-2 cells were plated at a density of 4×10^3 per well on 96-well plates. For testing the effect of AKT-MeTAG **1** on proliferation, MCF7, H9C2, HDF and HUVEC cells were plated at a density of 5×10^2 per well on 96-well plates. Indicated drugs were twofold serially diluted in duplicate in the medium of choice, and an equal volume (100 μL) of serial drug dilution was added to the plates with cells (100 μL/well). Plates were incubated at 37 °C for indicated time, followed by treatment with CCK-8 regent (NCM Biotech, China) for additional 4 h, and the absorbance values were read at 450 nm. Cell viability rate was recorded as the average OD value in indicated drug-group/average OD value in control group × 100%.

4.10. PSA, Tmprss2, NKX3.1, EGR2 and FOS mRNA level detection by RT-PCR

Total RNA of VCap or HCT116 cells was extracted with TRIzol and reversed by using a Reverse Transcription Reaction Kit (MBI

Fermentas, St. Leon-Rot, Germany). Then cDNA was amplified using specific primers. Primer sequences were listed as follows: PSA (forward primer 5′-GGTGACCAAGTTCATGCTGTG-3′, reverse primer 5′-GTGTCCTTGATCCACTTCCG-3′); Tmprss2 (forward primer 5′-CAAGTGCTCCAACTCTGGGAT-3, reverse primer 5′-R AACACACCGATTCTCGTCCTC-3′), NKX3.1 (forward primer 5′-CCCACACTCAGGTGATCGAG-3′, reverse primer 5′-GAGCTGCTTTCGCTTAGTCTT-3′), GAPDH (forward primer 5′-GAAGGTGAAGGTCGGAGT-3′, reverse primer 5′-CATGG GTGGAATCATATTGGAA-3′), FOS (forward primer CCGGGGATAGCCTCTCTTACT, reverse primer CCAGGTCC GTGCAGAAGTC), EGR2 (forward primer TCAACATTGACAT GACTGGAGAG, reverse primer AGTGAAGGTCTGGTT TCTAGGT).

4.11. Mass spectrometry analysis

Argine methylation sites were identification using Nano-LC−MS/MS equipped with electrospray ionization according to previously reported assay[63]. 293T cells were stably transfected with 10 μg HA-p300. 24 h after transfection, cells were treated with DMSO (control) or 20 μmol/L p300-MeTAG **1** for 24 h and lysed. For the identification of p300 methylation sites, the precipitates pulled down with anti-HA beads from 293T cells were first dissolved in denaturation buffer (8 mol/L urea and 0.1 mol/L Tris−HCl, pH 8.5). The solution was then centrifuged at 14,000×*g* for 20 min at 4 °C. Subsequently, the urea in the protein mixture was replaced with 50 mmol/L NH_4HCO_3 by centrifugation at 14,000×*g* for 20 min at 20 °C, repeated three times. The proteins were then digested overnight at 37 °C using sequencing-grade modified trypsin (Promega) at a protein-to-enzyme ratio of 50:1.

For the mapping of p300 arginine methylation, liquid chromatography-mass spectrometry (LC−MS) analysis was conducted using a nanoflow EASY-nLC 1000 system (ThermoFisher Scientific, Odense, Denmark) coupled with an Orbitrap Elite mass spectrometer (ThermoFisher Scientific, Bremen, Germany). The samples were analyzed on a C18 analytical column (75 μm i.d. × 20 cm, ReproSil-Pur 120 C18-AQ, 1.9 μm, Dr. Maisch GmbH, Germany). The mobile phases comprised solution A (0.1% formic acid) and solution B (0.1% formic acid in 100% acetonitrile). Peptide elution conditions: 5−28% solution B (50 min), 28%−90% solution B (2 min), and 90% solution B (10 min) at a flow rate of 200 nL/min, with the spray voltage at 2.0 kV, the heated capillary temperature at 275 °C. MS/MS experiments were performed in the Orbitrap using higher-energy collisional dissociation (HCD) fragmentation with an isolation window of 1.6 and a resolution of 15,000, employing a normalized collision energy (NCE) of 30%. The signal threshold was set at 5000, and the normalized collision energy was set to 35%. The resulting data were processed using the UniProt human protein database (70,956 entries, downloaded on December 2, 2016) with Protein Discoverer (Version 1.4.0.288, ThermoFisher Scientific) and Mascot (Version 2.3.2, Matrix Science). Mass tolerances were set to 10 ppm for precursors and 0.05 Da for fragment ions. The minimum precursor mass was set at 350 Da, with a maximum precursor mass of 8000 Da. Up to two missed cleavages were permitted. Carbamidomethylation of cysteine was specified as a fixed modification, while acetylation at the protein N-terminus, oxidation of methionine, and methylation of arginine were considered variable modifications. The false discovery rate (FDR) threshold for peptide identification was set at 0.05.

Acknowledgments

This work was supported in part by National Key R&D Program of China (No. 2023YFC3404104, China), National Natural Science Foundation of China (No. 82230097, China), National Natural Science Foundation of China (No. 82273128, China), and Institutional Foundation of the First Affiliated Hospital of Xi'an Jiaotong University (No. 2021QN-14, China).

Author contributions

Yanlin Jian: Investigation, Formal analysis, Data curation, Conceptualization. Tianyang Zhou: Methodology, Formal analysis, Data curation. Chendong Guo: Methodology, Investigation, Data curation. Yibo Gao: Software, Methodology, Investigation. Chen Yao: Investigation, Data curation. Zixi Wang: Visualization, Software. Xuehan Jiang: Methodology, Data curation. Ke Wang: Supervision, Data curation. Jian Ma: Project administration, Conceptualization. Yang Gao: Visualization, Validation, Supervision. Yizeng Fan: Data curation, Conceptualization. Jing Liu: Writing − review & editing, Supervision, Conceptualization. Bohan Ma: Investigation, Data curation, Conceptualization. Lei Li: Writing − review & editing, Validation, Supervision, Conceptualization.

Conflicts of interest

The authors declare no competing financial interest.

Appendix A. Supporting information

Supporting information to this article can be found online at https://doi.org/10.1016/j.apsb.2025.03.049.

References

1. Larsen SC, Sylvestersen KB, Mund A, Lyon D, Mullari M, Madsen MV, et al. Proteome-wide analysis of arginine monomethylation reveals widespread occurrence in human cells. *Sci Signal* 2016;**9**:rs9.
2. Peng C, Wong CCL. The story of protein arginine methylation: characterization, regulation, and function. *Expert Rev Proteomics* 2017;**14**:157−70.
3. Blanc RS, Richard S. Arginine methylation: the coming of age. *Mol Cell* 2017;**65**:8−24.
4. Yang YZ, Bedford MT. Protein arginine methyltransferases and cancer. *Nat Rev Cancer* 2013;**13**:37−50.
5. Hornbeck PV, Zhang B, Murray B, Kornhauser JM, Latham V, Skrzypek E. PhosphoSitePlus, 2014: mutations, PTMs and recalibrations. *Nucleic Acids Res* 2015;**43**:D512−20.
6. McBride AE, Silver PA. State of the arg: protein methylation at arginine comes of age. *Cell* 2001;**106**:5−8.
7. Bedford MT, Clarke SG. Protein arginine methylation in mammals: who, what, and why. *Mol Cell* 2009;**33**:1−13.
8. Mowen KA, David M. Unconventional post-translational modifications in immunological signaling. *Nat Immunol* 2014;**15**:512−20.
9. Jarrold J, Davies CC. PRMTs and arginine methylation: cancer's best-kept secret?. *Trends Mol Med* 2019;**25**:993−1009.
10. Kim HJ, Kim NC, Wang YD, Scarborough EA, Moore J, Diaz Z, et al. Mutations in prion-like domains in hnRNPA2B1 and hnRNPA1 cause multisystem proteinopathy and ALS. *Nature* 2013;**495**:467−73.
11. Ryan VH, Dignon GL, Zerze GH, Chabata CV, Silva R, Conicella AE, et al. Mechanistic view of hnRNPA2 low-complexity domain structure, interactions, and phase separation altered by mutation and arginine methylation. *Mol Cell* 2018;**69**:465−79.e7.

12. Sun Q, Fang L, Tang X, Lu S, Tamm M, Stolz D, et al. TGF-β upregulated mitochondria mass through the SMAD2/3→C/EBPβ→PRMT1 signal pathway in primary human lung fibroblasts. *J Immunol* 2019;**202**:37−47.
13. Huq MDM, Gupta P, Tsai NP, White R, Parker MG, Wei LN. Suppression of receptor interacting protein 140 repressive activity by protein arginine methylation. *EMBO J* 2006;**25**:5094−104.
14. Wang Y, Wysocka J, Sayegh J, Lee YH, Perlin JR, Leonelli L, et al. Human PAD4 regulates histone arginine methylation levels *via* demethylimination. *Science* 2004;**306**:279−83.
15. Yang C, Dong ZZ, Zhang J, Teng D, Luo X, Li D, et al. Peptidylarginine deiminases 4 as a promising target in drug discovery. *Eur J Med Chem* 2021;**226**:113840.
16. Zhu D, Lu Y, Yan Z, Deng Q, Hu B, Wang Y, et al. A β-carboline derivate PAD4 inhibitor reshapes neutrophil phenotype and improves the tumor immune microenvironment against triple-negative breast cancer. *J Med Chem* 2024;**67**:7973−94.
17. Wang L, Wen M, Cao X. Nuclear hnRNPA2B1 initiates and amplifies the innate immune response to DNA viruses. *Science* 2019;**365**: eaav0758.
18. Chang B, Chen Y, Zhao Y, Bruick RK. JMJD6 is a histone arginine demethylase. *Science* 2007;**318**:444−7.
19. Xiao RQ, Ran T, Huang QX, Hu GS, Fan DM, Yi J, et al. A specific JMJD6 inhibitor potently suppresses multiple types of cancers both *in vitro* and *in vivo*. *Proc Natl Acad Sci USA* 2022;**119**:e2200753119.
20. Walport LJ, Hopkinson RJ, Chowdhury R, Schiller R, Ge W, Kawamura A, et al. Arginine demethylation is catalysed by a subset of JmjC histone lysine demethylases. *Nat Commun* 2016;**7**:11974.
21. Branscombe TL, Frankel A, Lee JH, Cook JR, Yang ZH, Pestka S, et al. PRMT5 (Janus kinase-binding protein 1) catalyzes the formation of symmetric dimethylarginine residues in proteins. *J Biol Chem* 2001; **276**:32971−6.
22. Yang YZ, Hadjikyriacou A, Xia Z, Gayatri S, Kim D, Zurita-Lopez C, et al. PRMT9 is a Type II methyltransferase that methylates the splicing factor SAP145. *Nat Commun* 2015;**6**:6428.
23. Zurita-Lopez CI, Sandberg T, Kelly R, Clarke SG. Human protein arginine methyltransferase 7 (PRMT7) is a Type III enzyme forming ω—monomethylated arginine residues. *J Biol Chem* 2012;**287**:7859−70.
24. Fedoriw A, Rajapurkar SR, O'Brien S, Gerhart SV, Mitchell LH, Adams ND, et al. Anti-tumor activity of the Type I PRMT inhibitor, GSK3368715, synergizes with PRMT5 inhibition through MTAP loss. *Cancer Cell* 2019;**36**:100−14.
25. Yu J, Sun Y, Guo S, Wang HQ, Wu J, Jiang X, et al. A phase I study of safety, pharmacokinetics, and pharmacodynamics of SCR-6920, a protein arginine methyltransferase 5 (PRMT5) inhibitor, in patients with advanced malignant tumors. *Ann Oncol* 2023;**34**:S474.
26. Monga V, Johanns TM, Stupp R, Chandra S, Falchook GS, Giglio P, et al. A phase 1 study of the protein arginine methyltransferase 5 (PRMT5) brain-penetrant inhibitor PRT811 in patients (pts) with recurrent high-grade glioma or uveal melanoma (UM). *J Clin Oncol* 2023;**41**:3008.
27. Patel MR, Monga V, Jauhari S, Stevens D, Masarova L, McKean M, et al. A phase 1 dose escalation study of protein arginine methyltransferase 5 (PRMT5) inhibitor PRT543 in patients with myeloid malignancies. *Blood* 2021;**138**:2609−11.
28. Xu J, Richard S. Cellular pathways influenced by protein arginine methylation: implications for cancer. *Mol Cell* 2021;**81**:4357−68.
29. Bekes M, Langley DR, Crews CM. PROTAC targeted protein degraders: the past is prologue. *Nat Rev Drug Discov* 2022;**21**:181−200.
30. Henning NJ, Boike L, Spradlin JN, Ward CC, Liu G, Zhang E, et al. Deubiquitinase-targeting chimeras for targeted protein stabilization. *Nat Chem Biol* 2022;**18**:412−21.
31. Siriwardena SU, Munkanatta Godage DNP, Shoba VM, Lai S, Shi M, Wu P, et al. Phosphorylation-inducing chimeric small molecules. *J Am Chem Soc* 2020;**142**:14052−7.
32. Yamazoe S, Tom J, Fu Y, Wu W, Zeng L, Sun C, et al. Heterobifunctional molecules induce dephosphorylation of kinases—a proof of concept study. *J Med Chem* 2020;**63**:2807−13.
33. Wang WW, Chen LY, Wozniak JM, Jadhav AM, Anderson H, Malone TE, et al. Targeted protein acetylation in cells using heterobifunctional molecules. *J Am Chem Soc* 2021;**143**:16700−8.
34. Zhu Y, Hart GW. Dual-specificity RNA aptamers enable manipulation of target-specific *o*-GlcNAcylation and unveil functions of *o*-GlcNAc on β-catenin. *Cell* 2023;**186**:428−45.
35. Ma B, Khan KS, Xu T, Xeque Amada J, Guo Z, Huang Y, et al. Targeted protein *o*-GlcNAcylation using bifunctional small molecules. *J Am Chem Soc* 2024;**146**:9779−89.
36. Yin S, Liu L, Brobbey C, Palanisamy V, Ball LE, Olsen SK, et al. PRMT5-mediated arginine methylation activates AKT kinase to govern tumorigenesis. *Nat Commun* 2021;**12**:3444−56.
37. Huang L, Zhang XO, Rozen EJ, Sun X, Sallis B, Verdejo-Torres O, et al. PRMT5 activates AKT *via* methylation to promote tumor metastasis. *Nat Commun* 2022;**13**:3955−70.
38. Mounir Z, Korn JM, Westerling T, Lin F, Kirby CA, Schirle M, et al. ERG signaling in prostate cancer is driven through PRMT5-dependent methylation of the androgen receptor. *Elife* 2016;**5**:e13964-82.
39. Chan-Penebre E, Kuplast KG, Majer CR, Boriack-Sjodin PA, Wigle TJ, Johnston LD, et al. A selective inhibitor of PRMT5 with *in vivo* and *in vitro* potency in MCL models. *Nat Chem Biol* 2015;**11**:432−7.
40. *ClinicalTrials.gov.* https://clinicaltrials.gov/ct2/show/NCT02783300. [Accessed 13 December 2023].
41. Watson PA, Arora VK, Sawyers CL. Emerging mechanisms of resistance to androgen receptor inhibitors in prostate cancer. *Nat Rev Cancer* 2015;**15**:701−11.
42. Han X, Wang C, Qin C, Xiang W, Fernandez-Salas E, Yang CY, et al. Discovery of ARD-69 as a highly potent proteolysis targeting chimera (PROTAC) degrader of androgen receptor (AR) for the treatment of prostate cancer. *J Med Chem* 2019;**62**:941−64.
43. Alegre-Martí A, Jiménez-Panizo A, Martínez-Tébar A, Poulard C, Peralta-Moreno MN, Abella M, et al. A hotspot for posttranslational modifications on the androgen receptor dimer interface drives pathology and anti-androgen resistance. *Sci Adv* 2023;**9**:ade2175−eade2200.
44. Hu R, Lu CX, Mostaghel EA, Yegnasubramanian S, Gurel M, Tannahill C, et al. Distinct transcriptional programs mediated by the ligand-dependent full-length androgen receptor and its splice variants in castration-resistant prostate cancer. *Cancer Res* 2012;**72**:3457−62.
45. Thangapazham R, Saenz F, Katta S, Mohamed AA, Tan SH, Petrovics G, et al. Loss of the tumorsuppressor promotes the - fusion gene expression in prostate cancer. *BMC Cancer* 2014;**14**:1−12.
46. Bowen C, Zheng T, Gelmann EP. NKX3.1 Suppresses gene rearrangement and mediates repair of androgen receptor-induced DNA damage. *Cancer Res* 2015;**75**:2686−98.
47. Zoma M, Curti L, Shinde D, Albino D, Mitra A, Sgrignani J, et al. EZH2-induced lysine K362 methylation enhances TMPRSS2-ERG oncogenic activity in prostate cancer. *Nat Commun* 2021;**12**:4147−65.
48. Davies BR, Greenwood H, Dudley P, Crafter C, Yu DH, Zhang JC, et al. Preclinical pharmacology of AZD5363, an inhibitor of AKT: pharmacodynamics, antitumor activity, and correlation of monotherapy activity with genetic background. *Mol Cancer Therapeut* 2012;**11**:873−87.
49. Xu J, Yu XF, Martin TC, Bansal A, Cheung K, Lubin A, et al. AKT degradation selectively inhibits the growth of PI3K/PTEN pathway-mutant cancers with wild-type KRAS and BRAF by destabilizing aurora kinase B. *Cancer Discov* 2021;**11**:3064−89.
50. Zhang SK, Ma YQ, Hu XY, Zheng YH, Chen XK. Targeting PRMT5/Akt signalling axis prevents human lung cancer cell growth. *J Cell Mol Med* 2019;**23**:1333−42.
51. Liu F, Cheng GY, Hamard PJ, Greenblatt S, Wang L, Man N, et al. Arginine methyltransferase PRMT5 is essential for sustaining normal adult hematopoiesis. *J Clin Investig* 2015;**125**:3532−44.
52. Gong GQ, Bilanges B, Allsop B, Masson GR, Roberton V, Askwith T, et al. A small-molecule PI3Kα activator for cardioprotection and neuroregeneration. *Nature* 2023;**618**:159−68.
53. Weinert BT, Narita T, Satpathy S, Srinivasan B, Hansen BK, Schölz C, et al. Time-resolved analysis reveals rapid dynamics and broad scope of the CBP/p300 acetylome. *Cell* 2018;**174**:231−44.

54. Narita T, Ito S, Higashijima Y, Chu WK, Neumann K, Walter J, et al. Enhancers are activated by p300/CBP activity-dependent PIC assembly, RNAPII recruitment, and pause release. *Mol Cell* 2021;**81**: 2166−82.
55. Hay DA, Fedorov O, Martin S, Singleton DC, Tallant C, Wells C, et al. Discovery and optimization of small-molecule ligands for the CBP/p300 bromodomains. *J Am Chem Soc* 2014;**136**:9308−19.
56. Byun JS, Wong MM, Cui W, Idelman G, Li Q, De Siervi A, et al. Dynamic bookmarking of primary response genes by p300 and RNA polymerase II complexes. *Proc Natl Acad Sci USA* 2009;**106**:19286−91.
57. Chirnomas D, Hornberger KR, Crews CM. Protein degraders enter the clinic—a new approach to cancer therapy. *Nat Rev Clin Oncol* 2023; **20**:265−78.
58. Pergu R, Shoba VM, Chaudhary SK, Godage DNPM, Deb A, Singha S, et al. Development and applications of chimera platforms for tyrosine phosphorylation. *Acs Central Sci* 2023;**9**:1558−66.
59. Zhang QY, Wu XX, Zhang HH, Wu QY, Fu M, Hua LW, et al. Protein phosphatase 5-recruiting chimeras for accelerating apoptosis-signal-regulated kinase 1 dephosphorylation with antiproliferative activity. *J Am Chem Soc* 2022;**145**:1118−28.
60. Seabrook LJ, Franco CN, Loy CA, Osman J, Fredlender C, Zimak J, et al. Methylarginine targeting chimeras for lysosomal degradation of intracellular proteins. *Nat Chem Biol* 2024;**20**:1566−76.
61. Sarott RC, Gourisankar S, Karim B, Nettles S, Yang H, Dwyer BG, et al. Relocalizing transcriptional kinases to activate apoptosis. *Science* 2024;**386**:eadl5361.
62. Liu J, Hu X, Luo K, Xiong Y, Chen L, Wang Z, et al. USP7-based deubiquitinase-targeting chimeras stabilize AMPK. *J Am Chem Soc* 2024;**146**:11507−14.
63. Shen SM, Ji Y, Zhang C, Dong SS, Yang S, Xiong Z, et al. Nuclear PTEN safeguards pre-mRNA splicing to link Golgi apparatus for its tumor suppressive role. *Nat Commun* 2018;**9**:2392−406.